Journal of Alloys and Compounds 505 (2010) 619–622

Contents lists available at ScienceDirect

Journal of Alloys and Compounds

journal homepage: www.elsevier.com/locate/jallcom

Dopant effects on the structural, optical and electromagnetic properties in multiferroic $Bi_{1-x}Y_xFeO_3$ ceramics

Nguyen Van Minh*, Dao Viet Thang

Center for Nano Science and Technology, Hanoi National University of Education, 136 Xuan-Thuy Road, Hanoi, Viet Nam

ARTICLE INFO

Article history:
Received 26 February 2010
Received in revised form 15 June 2010
Accepted 16 June 2010
Available online 25 June 2010

Keywords:
Multiferroics
Raman spectroscopy
Magnetization

ABSTRACT

Multiferroic $Bi_{1-x}Y_xFeO_3$ ($x = 0.00, 0.05, 0.1, 0.15, 0.2$) ceramics were prepared by conventional solid-state-reaction method. X-ray diffraction measurement was carried out to characterize the crystal structure and to detect the impurities existing in these ceramics. The substitution of rare earth Y for Bi was found to decrease the impurity phase in $BiFeO_3$ ceramics. There is strong evidence that both lattice constants a and c of the unit cell unusually change at Y content of about $x = 0.10$. The effect of introducing Y^{3+} is shown to increase the optical band gap for doped sample $Bi_{1-x}Y_xFeO_3$. Additionally, the Raman measurement performed for the lattice dynamics study of $Bi_{1-x}Y_xFeO_3$ samples reveals a strong band centered at around 1150–1350 cm^{-1} which is associated with the resonant enhancement of two-phonon Raman scattering in the multiferroic $Bi_{1-x}Y_xFeO_3$ samples. The impedance spectroscopy indicates that, the Y dopant has improved the grain impedance. The enhancement of magnetization was observed in Y-doped samples compared to pure $BiFeO_3$.

1. Introduction

Ferroelectromagnetic materials, i.e. multiferroics, exhibit ferroelectric properties in combination with the ferromagnetic properties [1]. Additionally they exhibit the phenomenon called magnetoelectric coupling, i.e. magnetization induced by an electric field and electric polarization by a magnetic field. Recently, partial substitution of Bi^{3+} ions by lanthanides has been shown to improve ferroelectric properties and magnetization [2–5]. Zhang et al. [3] and Das et al. [5] suggested that La^{3+} substitution for Bi^{3+} eliminates impurity phases and destroys the cycloidal spin structure resulting in uniform canted antiferromagnetic ordering. Zhang et al. [3] also reported that the structure changes from rhombohedral to orthorhombic at 30 mol% La. In the studies on dopant effects of Sm reported by Nalwa et al. [2] and Yuan [6] and those of Nd reported by Yuan et al. [7] in $BiFeO_3$, changes in the crystal structure of the material were observed, which resulted in improved piezoelectric properties, long-range ferroelectric and canted antiferromagnetic orders. Uniyal and Yadav [8] claimed on the other hand, that 10 mol% Gd substituted for bismuth in the sample compound did not change the crystal structure but only reduced the volume fraction of impurity phases, while decreasing the Neel temperature T_N to ~150 °C from 370°C, and enhancing the magnetization to the extent of allowing the generation of the ferroelectric hysteresis loops [8]. These phenomena also give rise to unusual dynamical effects, which can be observed in optical experiment which offers the means for elucidating of the driving mechanism of the ferroelectric transition and, eventually, its coupling to magnetic ordering [9,10]. The origins of the ferroelectric order and its coupling to magnetic order, are closely related to the lattice dynamics which is in turn directly connected to ferroelectric order. The Raman spectroscopy is known to be a powerful tool for studying the vibrational and magnetic excitations [11]. Some studies on Raman scattering of $BiFeO_3$ have indeed been reported [12], but most of those studies were focused on pure $BiFeO_3$. Although a number of Raman and XRD experiments have also been performed to study the influence of temperature and dopant concentration variations, very little works have been reported on the Y dopant induced changes in the structure relating to optical property and to electromagnetic property of $BiFeO_3$. In this paper, we report the result of a study on the Y-doping effects in $Bi_{1-x}Y_xFeO_3$ by means of measurements and analyses of the XRD pattern as well as the Raman scattering, optical absorption spectra, impedance spectroscopy and magnetization.

2. Experiment

The $Bi_{1-x}Y_xFeO_3$ ($x = 0.00$, 0.05, 0.10, 0.15 and 0.20) samples were prepared by a modified solid-state-reaction method, which adopted a much faster heating and cooling rates in the sintering process than those employed in conventional method. The initial powder material for the synthesis was prepared by mixing appropriate amounts of Bi_2O_3 (Sigma–Aldrich, >99.0%), Y_2O_3 (Sigma–Aldrich, >99.9%) and Fe_2O_3 (Sigma–Aldrich, 99.9%), which were ground for 4 h in isopropyl alcohol. The powders were thereafter pressed into disks of 10 mm diameter and calcined at 600 °C for 6 h. The resulted pellets were further treated with a repeated grinding in isopropyl

* Corresponding author.
E-mail addresses: minhsp@gmail.com, minhnv@hnue.edu.vn (N.V. Minh).

0925-8388/$ – see front matter © 2010 Elsevier B.V. All rights reserved.
doi:10.1016/j.jallcom.2010.06.093

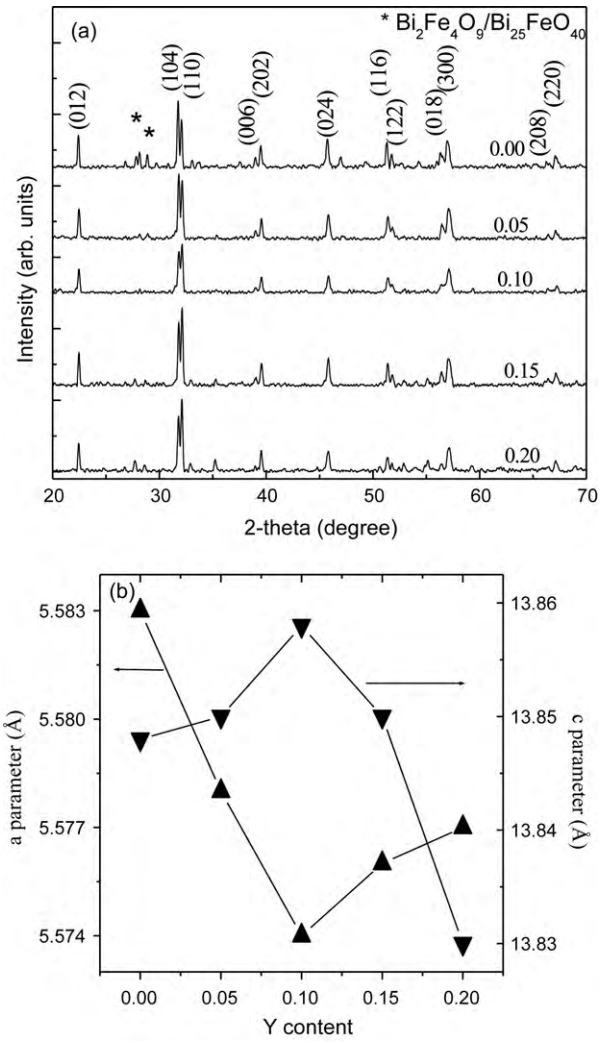

Fig. 1. (a) XRD patterns of $Bi_{1-x}Y_xFeO_3$ powders and (b) *a*, *c* cell parameters vs. Y content.

alcohol for 4 h. The powders were then pressed into disks of 10 mm in diameter and 5 mm in thickness, sintered at 825 °C for 10 h with heating rate of 10 °C/min and finally cooled at the rate of 5 °C/min.

Structural characterization was performed by means of X-ray diffraction using a D5005 diffractometer with Cu Kα radiation and with 2θ varied in the range of 20–70° at a step size of 0.02°. The photoabsorption of $Bi_{1-x}Y_xFeO_3$ was measured by UV–vis diffuse reflectance spectrometry (Jasco 670 UV–vis spectrometer). Raman measurements were performed in a back scattering geometry using Jobin Yvon T 64000 triple spectrometer equipped with a cryogenic charge-coupled device (CCD) array detector and operated with 514.5 nm line of Ar ion laser. The magnetization depending on magnetic field was measured by a vibrating sample magnetometer (VSM) and impedance spectroscopy was obtained by a Le Croy equipment.

3. Result and discussion

Fig. 1 shows the X-ray diffraction patterns of $Bi_{1-x}Y_xFeO_3$ (x = 0.05, 0.10, 0.15, 0.20). The XRD patterns are in excellent accord with the powder data of JCPDS Card No. 71-2494. Generally, for all samples, the second phase peaks attributed to Fe or Bi rich phases, $Bi_2Fe_4O_9$ and $Bi_{25}FeO_{40}$ (asterisk in Fig. 1a) were routinely observed as shown in previous results [13]. However, the remain peaks in the XRD traces are related to perovskite-structured phases, while the second phase peaks apparently disappear in the XRD data of sample with x = 0.10. For Y-doped $BiFeO_3$, all peaks are indexed according to the R_{3c} cell of $BiFeO_3$. The lattice parameters deduced for pure $BiFeO_3$ hexagonal unit cell were found to have values a = 5.5778 Å and c = 13.8685 Å. In the range of x = 0.00 to x = 0.10, the cell parameters increase with increasing Y content. Upon this content, the cell parameter decreases (Fig. 1b) indicating the smaller Y ions have indeed replaced the larger Bi ions in the unit cell.

The further effect of Y-substitution is described by the Raman spectra of the $Bi_{1-x}Y_xFeO_3$ ceramics which are plotted in Fig. 2 with respect to variation of Y concentration x at room temperature. The selection rules for the Raman active modes in rhombohedral $R_{3c}(C_{3v})$ symmetry predict only 13 active Raman phonons with A_1 and E symmetries, according to the rule of decomposition in terms of irreducible representations, $\Gamma_{Raman/IR} = 4A_1 + 9E$. In polarized Raman scattering, the A_1 modes can be observed by parallel polarization, while the E modes can be observed by both parallel and crossed polarizations. Since all these modes fall in the frequency range below ~700 cm^{-1}, most of the Raman studies have focused in this region, at the cost of missing the information contained at higher frequencies. Here, we measured the Raman spectra in the extended range of 100–1800 cm^{-1}. In addition to the well-understood Raman features in the low-frequency region, the spectra show a very prominent band at ~1000–1350 cm^{-1}, which we associate with two-phonon Raman scattering, strongly enhanced due to the resonance with the intrinsic absorption edge.

As seen from Fig. 2a, all samples show the same Raman modes at similar positions. When comparing the low-frequency Raman modes (100–700 cm^{-1}) with theoretical and experimental results reported previously [11], a reasonably good agreement is attained. The only difference is the appearance of a prominent additional band around ~1150–1350 cm^{-1} which has rarely been reported

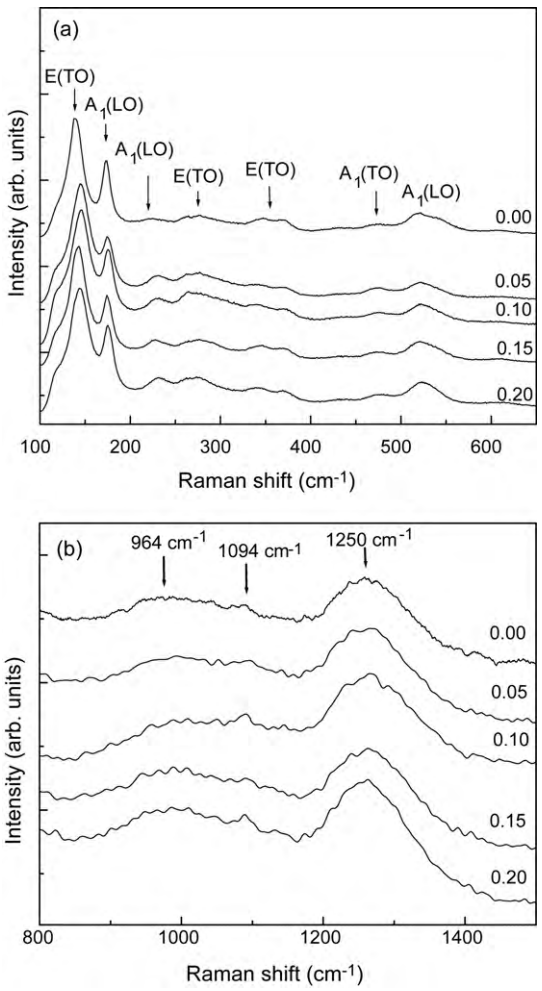

Fig. 2. The Raman spectra of $Bi_{1-x}Y_xFeO_3$ samples with x = 0.00–0.20.

before for the doped system. Changing the excitation wavelength to 488 nm led to no observable spectral shifts in this band, thereby confirming its true nature of Raman scattering and, excluding any possible phonon and/or magnon assisted emission in this region. The origin of this spectral band has been assigned to the combination of three different two-phonons Raman scattering in $BiFeO_3$ [14] labeled as $2A_4$, $2E_8$ and $2E_9$, since their spectral positions practically correspond to twice the energy values of the $A(LO_4) \sim 480\ cm^{-1}$, $E(TO_8) \sim 550\ cm^{-1}$ and $E(TO_9) \sim 620\ cm^{-1}$ normal modes of $BiFeO_3$, respectively. The strong contribution of the two-phonon band to the total Raman spectrum has been attributed to a resonant enhancement with the intrinsic absorption edge in $BiFeO_3$ (2.66 eV) [14,15]. In addition, the two-phonon Raman spectra are displayed in Fig. 2b. The slight difference and inconsistent variation in some of the peaks observed in the investigated samples can be attributed to the different subtle details in the sample preparations. It is known that the synthesis condition sensitively influences the oxygen stoichiometry of the resulted samples. This is expected to lead to changes in oxygen bonding and disorder that are reflected in the frequencies of vibration modes involving oxygen. Furthermore, it is reported that these high-frequency modes of $BiFeO_3$ are overtones of the first-order phonon modes and assigned as $2A_4$, $2E_8$, and $2E_9$ modes, respectively [16]. Some analysis was also discussed in this paper.

To elucidate the role of Y doped on the conductivity, we have measured the impedance of the samples. The impedance spectroscopy is usually used to characterize bulk grain, grain boundary and electrode interface contributions by exhibiting successive semicircles Cole–Cole plot (often with some distortion) with its imaginary part plotted against its real part in the complex plane [17,18]. A high-frequency semicircle originates from the bulk conduction and dielectric processes; a low-frequency semicircle is associated with ion and electron transfers at the contact surface between the sample and the electrode, while an intermediate-frequency semicircle provides information on the grain boundary and/or impurity-phase impedance. All these contributions vary with temperature, and, for a given frequency range of measurement, they may not all be detected.

For clarity, in Fig. 3 we show the Z''–Z' plots of the impedance of two samples ($x = 0.00$ and 0.20) together with the simulations results as most impedance investigations on polycrystalline samples with perovskite structure and other dielectric compounds, a series of parallel RC elements are used for the numerical simulation. Fig. 3a shows the plot for sample with $x = 0.00$ together with the simulated spectrum displaying a good fit. Here, the high-frequency semicircle seems to disappear. We attribute the semicircle at intermediate frequencies tentatively to grain boundaries.

The sample with a relatively high Y content might lead to high grain and low grain boundary resistivity (Fig. 3b). We note that in all cases, the simulated results fit the experimental data quite well.

It can be seen from Fig. 3, that there are two effects pertaining to microstructural inhomogeneity – grain and grain boundary. Impedance spectroscopy allows the separation of the resistance related to grains (bulk) and grain boundaries because each of them has different relaxation times. For sample with $x = 0.00$, the high-frequency semicircle originates from the bulk conduction and dielectric processes does not detect. Therefore, the spectrum reveals a relatively large grain boundary contribution to the total impedance [17,18]. The reason may be that close to the grain boundaries, the transport properties of the material are controlled by imperfections, expected to be present in higher concentration than in grains, leading to an additional contribution to the intergrain (grain boundary) impedance. The internal space charge created at the grain boundaries may lead to a significant increase in the concentration of mobile effects. Form above result, it was suggested that the Y dopant has improved the boundary impedance.

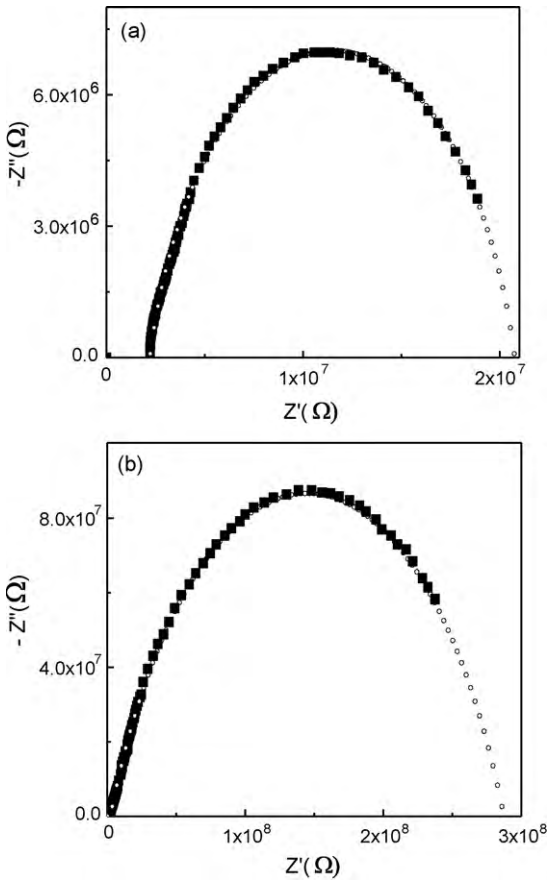

Fig. 3. Impedance spectroscopy of $Bi_{1-x}Y_xFeO_3$ samples with $x = 0.00$ (a) and $x = 0.20$ (b).

This is in agreement with the result of the calculated optical band gap data in previous part.

The magnetization–magnetic field (M–H) curves of $Bi_{1-x}Y_xFeO_3$ ceramics were measured with a maximum magnetic field of 10 kOe, as shown in Fig. 4. In fact, $BiFeO_3$ is known to be antiferromagnetic having a G-type magnetic structure [19], but has a residual magnetic moment due to a canted spin structure (weak ferromagnetic) [20]. However, the Y-doped specimens exhibited a magnetic hysteresis loop, referring to a ferromagnetic behavior. As shown

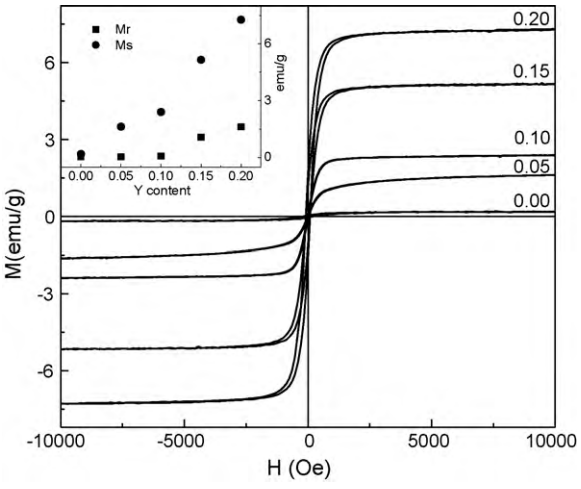

Fig. 4. Magnetization vs. magnetic field of $Bi_{1-x}Y_xFeO_3$ samples with $x = 0.00$–0.20. The inset is the saturation magnetization (M_s) and remanent magnetization (M_r) vs. Y content.

in Fig. 4, the curves of $x \geq 0.05$ are clearly not collinear. The saturation magnetization (M_s) are 1.62, 2.40, 5.16 and 7.27 emu/g for $x = 0.05$, 0.10, 0.15 and 0.20, respectively. The remnant magnetizations (M_r) are 0.04, 0.08, 1.07 and 1.62 emu/g, respectively. The M_s and M_r values as the function of x are plotted in the inset of Fig. 4. A relevant research [21] reported that the Y-substitution could suppress the spin cycloid of $BiYFeO_3$. Further analysis reveal that the M_s and M_r values of $Bi_{1-x}Y_xFeO_3$ with $x = 0.15$ and 0.20 are significantly bigger than those of others, suggesting that with $x < 0.10$, the Y-substitution can only suppress but cannot destruct the spin cycloid, which is responsible for the limited and smooth increase of the M_s and M_r values. However, when $x \geq 0.10$, the Y-substitution result in a structural phase transition wherein the spin cycloid may be destructed, so that the latent magnetization locked within the cycloid may be released, and a significant increased M_s and M_r values is observed. However, when $x \geq 0.10$, another phase, such as $Y_3Fe_5O_{12}$ can be found evidently, which also can contribute to the increase of magnetization value. Whether Y-substitution can improve the saturation magnetization so much should be discussed more and another effective analytical method should be introduced to assist.

4. Conclusion

In summary, the dopant induced changes in the structural, optical absorption, Raman scattering and electromagnetic properties of $Bi_{1-x}Y_xFeO_3$ samples have been investigated. It is shown that $Bi_{1-x}Y_xFeO_3$ crystallizes in the rhombohedral crystal structure at room temperature with the space group R_{3c}. The optical band gaps of $Bi_{1-x}Y_xFeO_3$ samples deduced from the UV–vis spectra indicate that, the optical band gap increases with increasing Y content. The Raman scattering measurement reveals a prominent two-phonon band around 1150–1350 cm^{-1}. Y dopant has improved the boundary impedance property of $Bi_{1-x}Y_xFeO_3$ samples. Weak ferromagnetism was observed in $Bi_{1-x}Y_xFeO_3$ powders at room temperature by using a vibrating sample magnetometer. The remanent magnetization and the saturation magnetization increase with Y-doping concentrations. Further studies will be needed to clarify the origin of the ferromagnetism in Y-doped $BiFeO_3$.

Acknowledgment

This work has been supported by The National Foundation for Science and Technology Development (NAFOSTED) of Vietnam (Code 103.06.14).

References

[1] W. Eerenstein, N.D. Mathur, J.F. Scott, Nature 442 (2006) 759.
[2] K.S. Nalwa, A. Grag, A. Upadhyaya, Mater. Lett. 62 (2008) 878.
[3] S.T. Zhang, et al., Appl. Phys. Lett. 88 (2006) 162901.
[4] Y.H. Lee, J.M. Wu, C.H. Lai, Appl. Phys. Lett. 88 (4) (2006) 042903.
[5] S.R. Das, et al., J. Appl. Phys. 101 (2007) 034104.
[6] G.L. Yuan, S.W. Or, J. Appl. Phys. 100 (2006) 024109.
[7] G.L. Yuan, Wing Siu, J.M. Liu, Z.G. Liu, Appl. Phys. Lett. 89 (2006) 052905.
[8] P. Uniyal, K.L. Yadav, Mater. Lett. 62 (17–18) (2008) 2858.
[9] B. Souchkov, J.R. Simpson, M. Quijada, H. Ishibashi, N. Hur, J.S. Ahn, S.W. Cheong, A.J. Millis, H.D. Drew, Phys. Rev. Lett. 91 (2003) 027203.
[10] A.P. Litvinchuk, M.N. Iliev, V.N. Popov, M.M. Gospodinov, J. Phys.: Condens. Matter. 16 (2004) 809.
[11] M. Cazayous, Y. Gallais, A. Sacuto, R. de Sousa, D. Lebeugle, D. Colson, Phys. Rev. Lett. 101 (2008) 037601, and references therein.
[12] Y. Yang, J.Y. Sun, K. Zhu, Y.L. Liu, J. Chen, X.R. Xing, Physica B 404 (2009) 171.
[13] J. Xu, G. Wang, H. Wang, D. Ding, Y. He, Mater. Lett. 63 (2009) 855–857; R. Mazumder, A. Sen, J. Alloy Compd. 475 (2009) 577–580.
[14] O. Mariola, M. Ramirez, S. Krishnamurthi, A. Denev, S.-Y. Kumar, Y.-H. Yang, E. Chu, J. Saiz, A. Seidel, P. Pyatakov, A. Bush, D. Viehland, J. Orenstein, R. Ramesh, V. Gopalan, Appl. Phys. Lett. 92 (2008) 022511.
[15] S.R. Basu, L.W. Martin, Y.H. Chu, M. Gajek, R. Ramesh, R.C. Rai, X. Xu, J.L. Musfeldt, Appl. Phys. Lett. 92 (2008) 091905.
[16] M.O. Ramirez, M. Krishnamurthi, S. Denev, A. Kumar, S.-Y. Yang, Y.-H. Chu, E. Saiz, J. Seidel, A.P. Pyatakov, A. Bush, D. Viehland, J. Orenstein, R. Ramesh, V. Gopalan, Appl. Phys. Lett. 92 (2008) 022511.
[17] E. Barsoukov, J. Ross Macdonald, Impedance Spectroscopy Theory, Experiment, and Applications, second edition, John Wiley & Sons, Inc, 2005, pp. 1–40.
[18] M. Zhu, H. Xie, J. Guo, W. Bai, Z. Xu, Sci. China 44 (2001) 336.
[19] A.J. Jacobson, B.E.F. Fender, J. Phys. C: Solid State Phys. 8 (1975) 844.
[20] S.V. Kiselev, R.P. Ozerov, G.S. Zhdanov, Sov. Phys. Dokl. 7 (1963) 742.
[21] R.K. Mishra, D.K. Pradhan, R.N.P. Choudhary, J. Phys.: Condens. Matter. 20 (2008) 045218.